

## Novel high performed and fouling resistant PSf/ZnO membranes for water treatment

Adem Sarihan<sup>\*1</sup> and Erdal Eren<sup>2</sup>

<sup>1</sup>Higher Vocational School, Bilecik Seyh Edebali University, 11210, Bilecik, Turkey

<sup>2</sup>Department of Chemistry, Faculty of Science and Arts, Bilecik Seyh Edebali University, 11210, Bilecik, Turkey

(Received August 19, 2016, Revised January 16, 2017, Accepted July 4, 2017)

**Abstract.** Antibacterial effective, high performed, novel ZnO embedded composite membranes were obtained by blending ZnO nanoparticles with polysulfone. IR, TG/DTG, XRD and SEM analysis were performed to characterize structure and morphology of ZnO nanoparticles and composite membranes. Contact angle, EWC, porosity and pore structure properties of composite membranes were investigated. Cross-flow filtration studies were performed to investigation of performances of prepared membranes. It was found from the cross section SEM images that ZnO nanoparticles dispersed homogenously up to additive amount of 2% and the membrane skin layer thicknesses increased in the presence of ZnO. Contact angle of pure PSf membranes were reduced from 70° to 55° after addition of 4% ZnO. Porosity of composite membrane contains 1% ZnO was higher about 22% than pure PSf membrane. BSA rejection ratio and PWF of 0.5% ZnO embedded composite membrane became 2.2 and 2.3 times higher than pure PSf membrane. It was determined from flux recovery ratios that ZnO additive increased the fouling resistance of composite membranes. Also, the bacterial killing ability of ZnO is well known and there are many researches related to this in the literature. Therefore, it is expected that prepared composite membranes will show antibacterial effect.

**Keywords:** membrane; ultrafiltration; water treatment; flux; antifouling

### 1. Introduction

Membrane filtration techniques are important and promising technologies for applications in water and waste water purification (Hong and He 2014). The performance of membranes depend on hydrophilicity, porosity, pore structure and fouling resistance properties (Padaki *et al.* 2011). Within many polymers, polysulfone is one of the most popular and suitable polymer, with good chemical and thermal stability, sufficient mechanical properties, easy film forming nature, low cost and commercial availability for ultrafiltration processes. However, PSf membranes exhibit drawback in filtration processes because of hydrophobic nature of PSf. Hydrophobic properties of PSf membranes simplifies membrane fouling. Among the several types of foulings like colloidal, organic and biological. Among the fouling types, biofouling is the most important problem (Vrouwenvelder *et al.* 2011). Because, biological foulants as well as the decreasing the pure water

---

\*Corresponding author, Ph.D., E-mail: [adem.sarihan@bilecik.edu.tr](mailto:adem.sarihan@bilecik.edu.tr)

flux and membrane performance, also reducing the life of membrane by disrupting the chemical structure.

A lot of different techniques were used to increase the antibacterial characteristics and hydrophilicity of the membranes. Recently studies on biofouling resistant membranes focused on blending of the membrane polymer with antibacteriyel effective nanoparticles, due to the simlicity, efficiency and cost-effectivity of the technique (Hong and He 2014).

In order to improve the performances of membranes, various nano materials, like  $\text{Al}_2\text{O}_3$ ,  $\text{SiO}_2$  (Cui *et al.* 2010), clay (Koh *et al.* 2010) and  $\text{TiO}_2$  (Damodara *et al.* 2009) have been used widely. Recently, ZnO nanoparticles attract significant attention because of their outstanding physical, chemical and environmentally friendly properties and excellent antibacterial effect (Balta *et al.* 2012, Yuan *et al.* 2010, Xie *et al.* 2011). Also ZnO nanoparticles have highly antibacterial activities against many bacteria and very little effect on human cells. Furthermore, ZnO nanoparticles can easily blend with polysulfone by dispersing with ultrasonication treatment in solvent, without any modification. Ultrafiltration membrane studies by using ZnO as an additive is still attractive. In our review of the literature, there is no enough data about to examination of ZnO nano particles on PSf membrane morphology and peformance. There are only a few articles in the literature about polysulfone ZnO composite membrane for water purification. The ones that exist are not enough in many directions. The nanoparticle ratios examined are not sufficient, no data about low amount of ZnO content. No investigation about average pore radius and water content. SEM analysis and images quite inadequate. No enough data about membrane antifouling ability like FRR. So this study is necessary to detailed investigate the effect of ZnO nanoparticles on the polysulfone membranes.

Therefore, the purpose of this work is to increase the antibacterial characteristics and filtration performances of the membranes blending with ZnO nanoparticles. Infrared spectroscopy (FTIR), X-ray diffraction (XRD) and thermal analysis (TGA) were used for the characterization of synthesized ZnO particles. To characterize pure PSf and ZnO embedded composite membranes, SEM, IR, TGA, DTG contact angle and filtration measurements were performed. Albumin (BSA) was used to determine the performances and fouling resistances of composite membranes.

## 2. Materials and methods

### 2.1 Materials

Polysufone ( $M_w=35.000\text{g/mol}$ ), 1-methyl-2-pyrrolidone (NMP), poly (ethylene glycol) (PEG-400), Oxalic acid:  $\geq 99.5\%$ , Ethanol:  $\geq 99.8\%$ ,  $\text{NaH}_2\text{PO}_4 \geq 99\%$ ,  $\text{Na}_2\text{HPO}_4 \geq 99\%$ , and Bovine Serum Albumin 66 kDa (BSA),  $\geq 98\%$  from Sigma Aldrich, Zinc acetate dihydrate 99%, from Ridel de Haen, was used in this study.

### 2.2 Preparation and characterization of ZnO nanoparticles

Appropriate amount of  $\text{Zn}(\text{OAc})_2 \cdot 2\text{H}_2\text{O}$  was added in absolute ethanol at  $60^\circ\text{C}$  (A). Oxalic acid dehydrate that was dissolved in ethanol at  $50^\circ\text{C}$  (B). B was added to A slowly with slightly mixing. After mixing of solutions, a white gel obtained and it was for dried at  $80^\circ\text{C}$ , then it was calcined at  $550^\circ\text{C}$  and ZnO nanoparticles were obtained (Hossaini-Sarvari 2011). XRD, FTIR, and TGA were used for the characterization of synthesized ZnO particles. Especially XRD patterns

proved the formation of ZnO nanoparticles

### 2.3 Preparation of membranes

For preparation of pure PSf membrane casting solution, PSf (1.7 g) was completely dissolved in solvent (NMP) (7.30 g) at 60°C and pore former (PEG400) (1.0 g) were mixed with the PSf solution, then the solution were stirred 60°C for one night. For preparation of PSf/ZnO composite membrane casting solutions, PSf (1.7 g) was completely dissolved in solvent (NMP) (3.0 g) at 60°C and pore former (PEG) (1.0 g) were mixed with the PSf solution (solution 1). ZnO (0.1, 0.25, 0.50, 1.0, 2.0, 3.0 and 4.0 g) were dispersed with ultrasonication treatment in certain amounts of NMP at 25°C for 1 h (frequency, 40 kHz, power 500 W) (solution 2). Then solution 2 were added to solution 1 then it was stirred at 60°C, for homogenously dispersion of the ZnO nanoparticles in PSf.

The phase inversion technique was used on preparation of pure and composite PSf membranes. First of all, the membrane casting solutions were casted on glass plate (15 cm×15 cm) using a hand-made casting knife. After 10 s, the glass plate immersed into the coagulation bath contains ultra pure water. A few secons later, phase inversion occurred, the film was separated from glass surface and the membranes obtained. The obtained membranes were kept in ultra pure water before performance tests. Casting solution compositions of the prepared membranes were shown in Table 1.

### 2.4 Characterization of membranes

Performance tests of the prepared composite membranes were performed by using cross-flow filtration cell which used our previous study (Eren *et al.* 2015).

KSV Attension contact angle meter was used to determine the water contact angles of membranes. To minimize errors all measurements were performed three times. Spectrum-100 FTIR spectrometer was used to FTIR analysis of the membranes, under air atmosphere. Seiko Exstar 7200 thermal analyser was used to thermal analysis. The morphologies of membranes were investigated by using SEM technique by using Zeiss GeminiSEM with coating platinum. BSA concentrations were determined with UV-vis spectrometer (PG instruments, T80. Spectrometer at  $\lambda_{max}$ =280 nm wavelength.

Table 1 Casting solution compositions of PSf/ZnO composite membranes

Membrane	Casting solution (% k/k)			
	PSf	NMP	PEG400	ZnO
Z0	17	73.0	10	0
Z1	17	72.90	10	0.1
Z2	17	72.75	10	0.25
Z3	17	72.50	10	0.5
Z4	17	72.0	10	1.0
Z5	17	71.5	10	1.5
Z6	17	70.0	10	3.0
Z7	17	69.0	10	4.0

### 2.4.1 Water content and porosity

Membrane porosity and water content (EWC) were examined by using wet-dry weight technique. Using the dry and wet weights of the membranes, EWC and porosity percents were calculated using Eqs. (1) and (2) respectively.

$$\text{Porosity (\%)} = \frac{A_w - A_d}{d \cdot V} \times 100 \quad (1)$$

$$\text{EWC (\%)} = \frac{A_w - A_d}{A_w} \times 100 \quad (2)$$

where  $W_w$  and  $W_d$  are the wet and dry membrane weight,  $d$  is the density of water at 25°C and  $V$  is the volume of membrane ( $\text{cm}^3$ ).

### 2.4.2 Pure Water Flux and average pore radius

PWFs of the membranes were determined by measurement of the permeate flux ( $\text{L}/\text{m}^2 \cdot \text{h}$ ), at different operating pressure such as 150, 200, 250 and 300 kPa by using Eq. (3), after the compaction of membranes. The membrane average pore radius were determined by using Guerout-Elford-Ferry equation (Liao *et al.* 2012) (Eq. (4)).

$$J_w = \frac{Q}{A \cdot \Delta t} \quad (3)$$

$$r_m = \sqrt{\frac{(2,9 - 1,75\varepsilon) \times 8\eta l Q}{\varepsilon \times A \times \Delta P}} \quad (4)$$

Here,  $r_m$  is average pore radius,  $\varepsilon$  is porosity data,  $\eta$  is viscosity of pure water ( $8,9 \times 10^{-4} \text{ Pa} \cdot \text{s}$ ),  $l$  is thickness of membrane (m),  $Q$  is water flux rate ( $\text{m}^3/\text{s}$ ),  $A$  is membrane working area of and  $\Delta P$  is the operation pressure (Pa).

### 2.4.3 Rejection and fouling resistance performance

BSA was used to investigation of the rejection performance of membranes. For this purpose, BSA was dissolved in phosphate buffer solution and concentrations were adjusted as  $500 \text{ mg L}^{-1}$  for all experiments. Furthermore, to determine the effect of pH on rejection, some rejection experiments were performed with BSA, at different pH values in Britton-Robinson buffer solutions. The working pH values were determined as isoelectric point of BSA (4.8), more acidic (3.0) and more basic (9.0). The rejection ratios were determined with the Eq. (5).

$$R (\%) = \left( 1 - \frac{C_p}{C_f} \right) \times 100 \quad (5)$$

In this equation,  $C_f$  and  $C_p$  symbolize the BSA concentrations in the feed and permeate, respectively.

Fouling resistance of the membranes examined with flux recovery ratio, which calculated by using Eq. (6).

$$\text{FRR (\%)} = \left( \frac{J_{w2}}{J_{w1}} \right) \times 100 \quad (6)$$

where, where  $J_{w2}$  and  $J_{w1}$  is the pure water flux of membranes after and before BSA rejection performances, respectively.

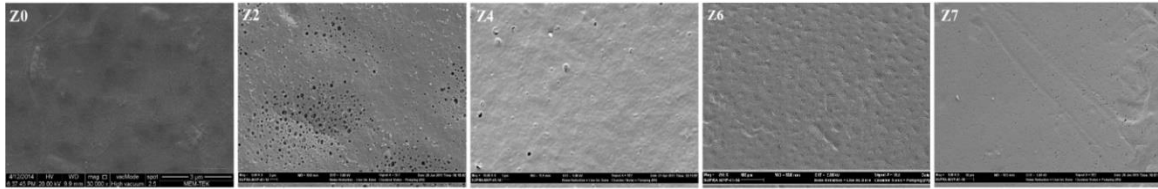


Fig. 1 Surface SEM images of some PSf/ZnO composite membranes

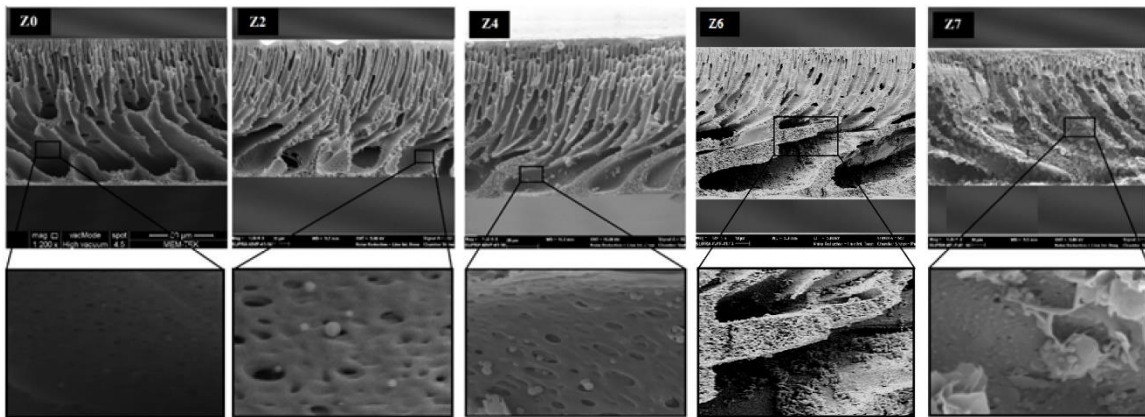


Fig. 2 Cross-sectional SEM images of some PSf/ZnO composite membranes

### 3. Result and discussion

#### 3.1 SEM analysis

SEM analysis were performed to investigate the influence of the ZnO additive on the PSf membrane morphology. Figs. 1 and 2 presents the top and cross-section SEM images of some composite membranes prepared with different ratio of ZnO nanoparticles. All membranes had similar surface properties. ZnO additive provided porous surfaces at 0.25% (Z2). But further increase of added ZnO nanoparticles to 0.5%, decreased the formation of pores (Z4). Addition of 4% ZnO supported the formation of dense and nonporous structure, due to increase in viscosity of the casting solution. Because, increasing the nanoparticle amount, decreased the amount of solvent in the casting solution, which were shown in Table 1. Hence an increase in the amount of nanoparticles effected the morphology and pore structure of membranes indirectly by changing the phase inversion speed. Because, more viscous casting solution results in slower phase inversion proces. There were many ZnO nanoparticles or aggregates on the surface of Z2 and Z4 membranes. However, the particles were rarely seen on Z6 and Z7 membrane, because nanoparticles were trapped in the dense structure which were seen clearly on cross-section SEM images of Z6 and Z7. The cross-section SEM images showed that all membranes exhibited dense skin layer, finger like pores and sponge like sublayer. The skin and sub layer thicknesses of 0.1-1.0% ZnO composite membranes were increased with increasing ZnO amounts. However, with the addition of 4%ZnO into the membrane casting solution, the length of the finger-like pores were decreased and cross-sectional structure of membrane turned into from finger-like to sponge like (Z6 and Z7). The main reason of the formation of dense structure was slow phase inversion

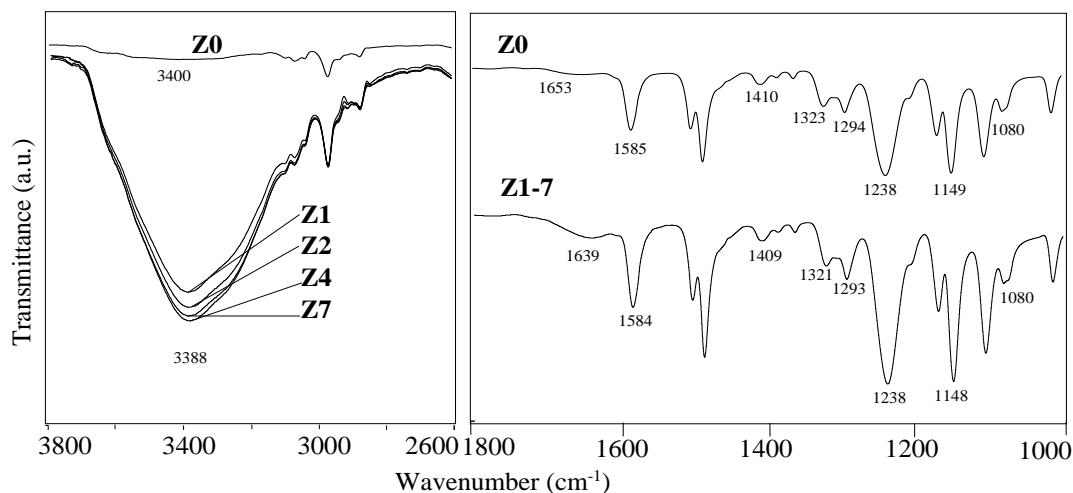


Fig. 3 IR spectras of PSf/ZnO composite membranes on different regions

resulting from the formation of viscose casting solution. It was shown in Z2 and Z4 cross section SEM images, ZnO nanoparticles dispersed homogeneously in the pores at low ratios but higher additive ratios, homogeneity was broken and agglomeration occurred which were seen on cross-section SEM images of Z6 and Z7. Also as it was seen in SEM images of Z2 and Z4 there were lots of nano holes in the pores. Formation of these holes may be related the mobility of nanoparticles in casting solution during the phase inversion process. On the other hand, when the dimensions of nanoparticles in the pores were examined, it was seen that the nanoparticles were nano sized about 100-500 nm.

### 3.2 FTIR analysis

FTIR studies were performed to identify the chemical structure of the composite membranes that contain various amount of ZnO. In the FTIR spectrum of the Z0, the bands at 1294 and 1149  $\text{cm}^{-1}$  represents the O=S=O groups of PSf. The characteristic band of C=C conjugation of the benzene ring was seen at 1585  $\text{cm}^{-1}$  (Ganesh *et al.* 2013, Padaki *et al.* 2010). Also, there were low intensity bands at nearly 3400 and 1650  $\text{cm}^{-1}$  indicating, OH stretching and bending frequencies. In the IR spectrum of ZnO additive composite membranes, it was seen that OH stretching and bending bands shifted to low frequencies and increased their intensity distinctly. This increasing showed the strong water absorption and high hydrophilicity of composite membranes. Also, O=S=O symmetric stretching and C=C conjugation bands shifted to lower frequencies (Fig. 3). This shiftings indicated the presence of interactions between PSf and ZnO nanoparticles. This results proves the good miscibility of ZnO nanoparticles and PSf.

### 3.3 TGA studies

Thermal stability of PSf/ZnO composite membranes were investigated by using TGA results. TGA curves of pure and composite membranes were shown in Fig. 4. TG/DTG datas were given in Table 2 where  $T_{\text{onset}}$  indicate the beginning temperature and  $T_{\text{max}}$  the temperature at the

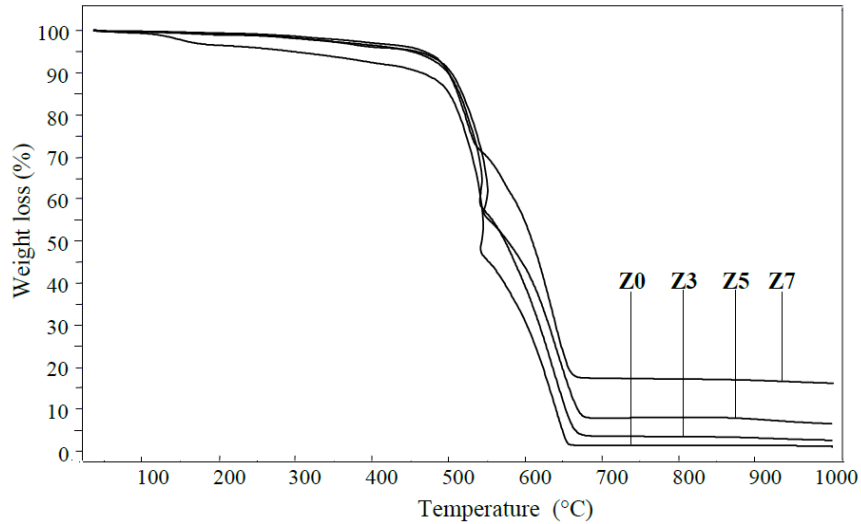


Fig. 4 TG curves of PSf/ZnO composite membranes

Table 2 Thermal analysis characteristics of some composite membranes.

	Z0	Z1	Z3	Z5	Z7
$T_{onset}$ (°C)	431	450	423	428	416
$T_{max1}$ (°C)	542	542	537	545	516
$T_{max2}$ (°C)	634	638	621	636	624
$(da/dt)_{max1}$ (%/min)	21.0	20.7	18.1	16.5	5.93
$(da/dt)_{max2}$ (%/min)	5.94	6.09	5.79	5.50	6.67

maximum weight-loss rate,  $(da/dt)_{max}$  represents maximum weight-loss rate, 1 and 2 indicate the first and second degradation stages. It was shown in the curves the amount of the residues increased with the ZnO additive ratio. Three different weight losses were observed for all membranes. The first around the 100°C is related to desorption of adsorbed water and residual solvent in membrane structure. Other two weight losses occur after 500°C which were attributed to the main chain polymer degradation. Compared to pure PSf membrane, ZnO composite membranes embedded ZnO nanoparticles show slightly lower thermal stability. This decrease in degradation temperatures could be explained by entering the nanoparticles between the polymer chain and reduce the interaction between chains. When the beginning decomposition temperatures were examined, it was seen that 0.1% ZnO added membrane surprisingly showed higher thermal stability than both composite and pure PSf membranes (Table 2). The cause of this result related with more homogenous dispersion of low amount nanoparticles in casting solution. Also, degradation rates on  $T_{max1}$  were decreased with the increasing amount of ZnO in PSf. This can be explain fast degradation of pure PSf structure due to its higher asymmetry. After addition of ZnO assymetry of PSf lost and degradation rate decreased.

### 3.4 Porosity, average pore radius, water content and contact angle analysis

Porosity, equilibrium water content and contact angle analysis results were given in Table 3

Table 3 Some characterization results of membranes

Membrane	Porosity (%)	Pore radius (nm)	Equilibrium water content (EWC) (%)	Contact angle (°)
Z0	62±1.9	26±0.9	74±2.4	70±1.4
Z1	73±1.8	26±1.2	78±1.4	66±1.2
Z2	75±1.6	35±1.9	80±1.9	-
Z3	76±1.2	22±1.0	79±1.7	63±1.1
Z4	73±1.5	28±2.2	75±2.7	-
Z5	69±1.8	29±1.3	77±1.8	55±0.9
Z6	69±2.1	24±1.6	76±1.2	-
Z7	50±2.9	28±1.0	75±1.4	55±1.4

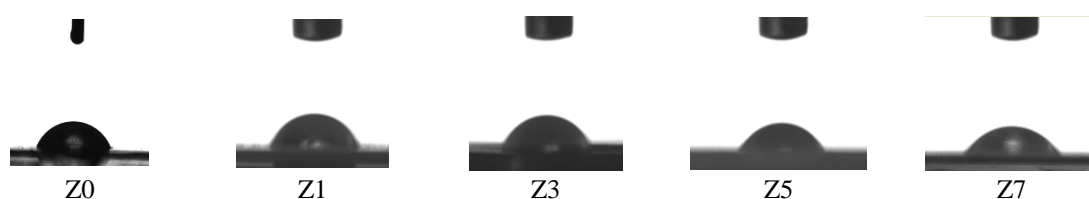


Fig. 5 Contact angle pictures of surface of some composite membrane

and contact angle images were shown in Fig. 5. The porosity of ZnO embedded composite membranes increased up to the additive amount of 0.5% (Z3) then decreased at higher additive ratios. As shown in SEM images, low amount ZnO embedded membrane structure has finger-like pores and nano-sized holes which were effective increase in porosity. At higher additive amounts, membrane structures turned from finger-like to sponge like, homogeneity of nanoparticles was broken, agglomeration occurred and also, the holes that occurred by the mobility of the nanoparticles in the casting solution during the phase inversion, blocked by nanoparticles, which were seen in SEM images, thus, the porosity of the membranes with higher amount of nanoparticles slightly lowered. Average pore radius of pure and composite membranes were similar and generally between 22-35 nm. EWC and contact angle is the most important properties for determination of membrane hydrophilicity. EWC and contact angle were used to determination of membrane general and surface hydrophilicity, respectively. As shown in Table 3 and Fig. 5, ZnO additive decreased the contact angle linearly so increased the membrane surface hydrophilicity. Also, it was seen from EWC results, all composite membranes had more hydrophilicity than pure PSf membrane.

### 3.5 Pure water flux, rejection and flux recovery ratio tests

Pure water flux (PWF) is very important parameter about membrane performance, because increasing the flux means decreasing the energy and cost. The pure water fluxes at 200 kPa, BSA rejection ratios and flux recovery ratios were given in Table 4. Also pure water fluxes of pure and composite membranes on different pressures were represented in Fig. 6. PWF of Z0 membrane increased 228 to 520 L/m<sup>2</sup>.h after addition of 0.5% ZnO at 200 kPa then decreased higher additive ratios. All composite membranes except Z6 and Z7 have higher PWF than pure PSf membrane at all pressures. High surface hydrophilicity, long finger-like pore structure and nano holes in the pores of Z1-Z5 composite membranes were effective in the increase in PWF. Decreasing the

Table 4 Some performance characteristics of composite membranes

Membrane	PWF (200 kPa) (L/m <sup>2</sup> .h)	BSA rejection (%)	FRR (%)
Z0	228±8	35.7±2.0	78±2.8
Z1	470±6	71.0±2.0	94±3.3
Z2	492±11	70.2±1.7	96±3.0
Z3	522±16	77.0±3.1	91±2.2
Z4	434±12	73.4±1.8	93±4.1
Z5	290±7	64.0±2.2	93±4.4
Z6	60±10	54.0±2.4	87±1.9
Z7	86±11	28.7±1.8	84±1.5

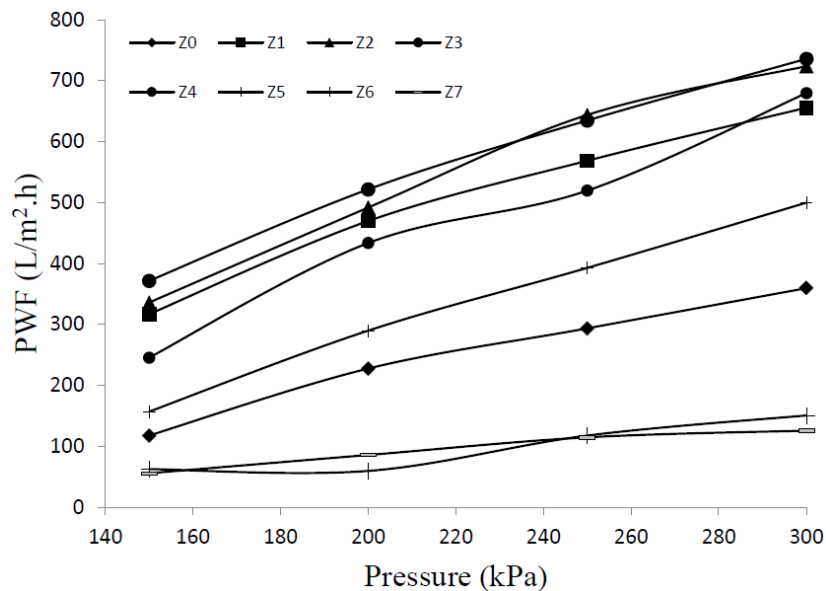


Fig. 6 Pure water flux performances of PSf/ZnO composite membranes

length of finger-like pores, dense sponge-like structure formation, and agglomeration of ZnO nanoparticles in pores blocking the nano holes were the most important reasons of the decreasing PWF on Z6 and Z7 membrane. Because there has been no significant decreasing in membrane porosities, but PWF results decreased significantly. Similarly PWF results, BSA rejection performances of composite membranes were increased up to the ZnO amount of 0.5% than decreased at higher ZnO ratios. The top skin layer thicknesses of membranes effected the rejection performances. As seen in the SEM images, the top skin layer thicknesses of ZnO embedded composite membranes increased Z1-Z4 membranes but decreased at higher additive ratios (Z6 and Z7). Thus, the decreasing the top skin layer thicknesses decreased the rejection performances of membranes. Determination of flux recovery ratio (FRR) is the best method to investigating the fouling resistance property of the membranes. It was seen at the Table 4 that FRR of Z0 membrane was 78% and all of the composite membranes had higher FRR than Z0 membrane. Because, owing to the hydrophilic nature of composite membranes, interactions between membrane and BSA were weakened so, fouling resistance of membranes increased.

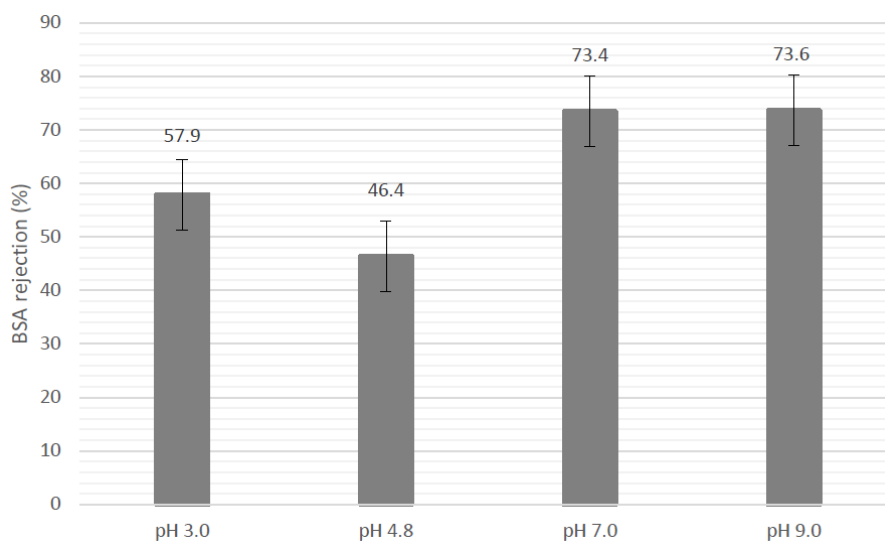


Fig. 7 BSA rejection performances of PSf/ZnO composite membranes at different solution pH

Table 5 Comparison of PSf/ZnO composite membranes with literature.

Membrane type	PWF (L/m <sup>2</sup> h)	BSA rejection (%)	FFR (%)	Contact angle (°)	Reference
% 1.0 ZnO blended PSf	-	93	-	78	(Leo <i>et al.</i> 2012)
~% 0.4 ZnO blended PES*	125 (at 100 kPa)	96	-	75	(Shen <i>et al.</i> 2012)
% 1.25 ZnO blended PES*	317 (at 100 kPa)	96	82	58	(Ahmad <i>et al.</i> 2015)
% 0.1 ZnO blended PSf	~5.3	-	-	59	(Alhoshan <i>et al.</i> 2013)
% 0.5 ZnO blended PSf	522 (at 200 kPa)	77	91	63	In this study

\* PES=Polyethersulfone

### 3.6 pH dependence of BSA rejection

BSA rejection studies at different pH values were performed to examine the effect of pH on BSA rejection. Polysulfone membrane surface negatively charged at a pH of 3 and higher pH (Nabe *et al.* 1997, Teng *et al.* 2006, Zularisam *et al.* 2007). ZnO nanoparticles has positively charge at a pH of 9 and lower pH (Ba-Abbad *et al.* 2010). Rejection results which were presented in Fig. 7 showed that the lowest rejection obtained at isoelectric point of BSA (4.8), because, the net charge on BSA was zero and electrical interctions between membrane and BSA were the lowest level at this pH. At the pH of 3, while membrane was positively charged, BSA was negatively charged therefore through electrical attraction, BSA was deposited in membrane pores and rejection performance a bit increased. As it was shown in Fig. 7, at the pH of 7 and 9, rejection of BSA significantly increased because, both membrane and BSA was negatively charged so electrical repulsion occurred.

### 3.7 Comparison of the PSf/ZnO membranes with literature

When we analyze the literature, it was seen there is only two article about PSf/ZnO composite

membranes and only two article about PES/ZnO composite membranes. The comparison of some characteristics of the prepared Z3 membrane with literature was given in Table 5. The results showed that BSA rejection of Z3 membrane is slightly lower than literature but 77% is still acceptable level for ultrafiltration. PWF, FRR and Contact angle of Z3 membrane is fairly high level. Compared to literature our study is more comprehensive research.

#### 4. Conclusions

In this study, phase inversion technique were used for the preparation of ZnO embedded PSf membranes. Morphologies and performances of prepared membranes were investigated and compared with pure PSf membrane. The results from this study showed that when used in appropriate amounts, ZnO additive improved many features of membranes. Porosity and equilibrium water content of membranes increased up to 21% and 8% after addition of ZnO nanoparticles. The contact angle of pure PSf membrane which was 70°, decreased with increasing ZnO amount and became 55° on 4% ZnO embedded membrane. With the addition of ZnO, the flux and rejection performances of membranes became higher about 2.3 and 2.2 times. Also, pH dependence of BSA rejection were investigated and it was determined that due to electrical repulsion forces between BSA and membrane surfaces rejection was increased. Flux recovery ratios of ZnO embedded membranes higher than pure PSf membrane's result and it means that ZnO additive increased the fouling resistance of membrane.

#### Acknowledgements

We thank TUBITAK, "Scientist Support Department" for supporting by 2211-C Scholarship Programme.

#### References

- Ahmad, A.L., Abdulkarim, A.A., Ismail, S. and Ooi, B.S. (2015), "Preparation and characterisation of PES-ZnO mixed matrix membranes for humic acid removal", *Desalin. Water. Treat.*, **54**(12), 3257-3268.
- Alhoshan, M., Alam, J., Dass, L.A. and Al-Homaidi, N. (2013), "Fabrication of polysulfone/ZnO membrane: influence of ZnO nanoparticles on membrane characteristics", *Adv. Polym. Tech.*, **32**(4), 21369.
- Ba-Abbad, M.M., Kadhum, A.A.H., Mohamad, A.B., Takriff, M.S. and Sopian, K. (2013), "Visible light photocatalytic activity of Fe<sup>3+</sup>-doped ZnO nanoparticle prepared via sol-gel technique", *Chemosph.*, **91**(11), 1604-1611.
- Balta, S., Sotto, A., Luis, P., Benea, L., Van der Bruggen, B. and Kim, J. (2012), "A new outlook on membrane enhancement with nanoparticles: the alternative of ZnO", *J. Membr. Sci.*, **389**, 155-161.
- Cui, A., Liu, Z., Xiao, C. and Zhang, Y. (2010), "Effect of micro-sized SiO<sub>2</sub>-particle on the performance of PVDF blend membranes via TIPS", *J. Membr. Sci.*, **360**(1-2), 259-264.
- Damodara, R.A., You, S.J. and Chou, H.H. (2009), "Study the self cleaning, antibacterial and photo catalytic properties of TiO<sub>2</sub> entrapped PVDF membranes", *J. Hazard. Mater.*, **172**(2-3), 1321-1328.
- Eren, E., Sarihan, A., Eren, B., Gumus, H. and Ozdemir Kocak, F. (2015), "Preparation, characterization and performance enhancement of polysulfone ultrafiltration membrane using PBI as hydrophilic modifier", *J.*

- Membr. Sci.*, **475**, 1-8.
- Ganesh, B.M., Isloor, A.M. and Ismail, A.F. (2013), "Enhanced hydrophilicity and salt rejection study of graphene oxide-polysulfone mixed matrix membrane", *Desalinat.*, **313**, 199-207.
- Hong, J. and He, Y. (2014), "Polyvinylidene fluoride ultrafiltration membrane blended with nano-ZnO particle for photo-catalysis self-cleaning", *Desalinat.*, **332**(1), 67-75.
- Hosseini-Sarvari, M. (2011), "Synthesis of quinolines using nano-flake ZnO as a new catalyst under solvent-free conditions", *J. Iran. Chem. Soc.*, **8**, 119-128.
- Koh, M.J., Hwang, H.Y., Kim, D.J., Kim, H.J., Hong, Y.T. and Nam, S.Y. (2010), "Preparation and characterization of porous PVDF-HFP/clay nano composite membranes", *J. Mater. Sci. Technol.*, **26**(7), 633-638.
- Leo, C.P., Lee, W.P.C., Ahmad, A.L. and Mohammad, A.W. (2012), "Polysulfone membranes blended with ZnO nanoparticles for reducing fouling by oleic acid", *Sep. Purif. Technol.*, **89**, 51-56.
- Liao, C., Zhao, J., Yu, P., Tong, H. and Luo, Y. (2012), "Synthesis and characterization of low content of different SiO<sub>2</sub> materials composite poly (vinylidene fluoride) ultrafiltration membranes", *Desalinat.*, **285**, 117-122.
- Nabe, A., Staude, E. and Belfort, G. (1997), "Surface modification of polysulfone ultrafiltration membranes and fouling by BSA solutions", *J. Membr. Sci.*, **133**(1), 57-72.
- Padaki, M., Isloor, A.M. and Wanichapichart, P. (2011), "Polysulfone/N-phthaloyl chitosan novel composite membranes for salt rejection application", *Desalinat.*, **279**(1), 409-414.
- Padaki, M., Isloor, A.M., Nagaraja, K.K., Nagaraja, H.S. and Pattabi, M. (2011), "Conversion of microfiltration membrane into nanofiltration membrane by vapour phase deposition of aluminium for desalination application", *Desalination*, **274** (1-3), 177-181.
- Shen, L., Bian, X., Lu, X., Shi, L., Liu, Z., Chen, L., Hou, Z. and Fan, K. (2012), "Preparation and characterization of ZnO/Polyethersulfone (PES) hybrid membranes", *Desalinat.*, **293**, 21-29.
- Teng, M.Y., Lin, S.H., Wu, C.Y. and Juang, R.S. (2006), "Factors affecting selective rejection of proteins within a binary mixture during cross-flow ultrafiltration", *J. Membr. Sci.*, **281**(1-2), 103-110.
- Vrouwenvelder, J.S., Van Loosdrecht, M.C.M. and Kruithof, J.C. (2011), "A novel scenario for biofouling control of spiral wound membrane systems", *Water Res.*, **45**(13), 3890-3898.
- Wang, X.M., Li, X.Y. and Shih, K. (2011), "In situ embedment and growth of anhydrous and hydrated aluminum oxide particles on polyvinylidene fluoride (PVDF) membranes", *J. Membr. Sci.*, **368**(1-2), 134-143.
- Xie, Y., He, Y., Irwin, P. L., Jin, T. and Shi, X. (2011), "Antibacterial Activity and Mechanism of Action of Zinc Oxide Nanoparticles against *Campylobacter jejuni*", *Appl. Environ. Microb.*, **77**(7), 2325-2331.
- Yuan, Q., Hein, S. and Misra, R.D.K. (2010), "New generation of chitosan-encapsulated ZnO quantum dots loaded with drug: Synthesis, characterization and in vitro drug delivery response", *Acta Biomater.*, **6**(7), 2732-2739.
- Zularisam, A.W., Ismail, A.F., Salim M.R., Sakinah, M. and Hiroaki, O. (2007), "Fabrication, fouling and foulant analyses of asymmetric polysulfone (PSF) ultrafiltration membrane fouled with natural organic matter (NOM) source waters", *J. Membr. Sci.*, **299**(1-2), 97-113.